A triboelectric gait sensor system for human activity recognition and user identification

Jiarong Li [a,b,1], Zixuan Xie [a,1], Zihan Wang [a,1], Zenan Lin [a], Chengyue Lu [a], Zihao Zhao [a], Yuchao Jin [a], Jihong Yin [a], Shilong Mu [a], Chaobo Zhang [b], Weihua Gui [b,d], Xiaojun Liang [b,*], Jiyu Wang [a,*], Wenbo Ding [a,b,c,**]

[a] Tsinghua-Berkeley Shenzhen Institute, Tsinghua Shenzhen International Graduate School, Tsinghua University, Shenzhen 518055, China
[b] Department of Mathematics and Theories, Peng Cheng Laboratory, Shenzhen 518055, China
[c] RISC-V International Open Source Laboratory, Shenzhen 518055, China
[d] School of Automation, Central South University, Changsha 410083, China

ARTICLE INFO

ABSTRACT

Floor-based sensing systems to monitor human activities and identify users are essential for smart homes and intelligent buildings. A low-cost, easy-to-fabricate, and flexible gait sensor system based on triboelectric nano-generator (TENG) is presented in this paper, which can transform gait movements, even in the low-frequency form, into electrical impulses without an external power source. To realize this, a TENG-based gait sensor unit with an optimized structure design is proposed to enhance the sensing sensitivity. A sensing insole module is formed by arranging the sensor units according to the foot pressure distribution. The sensor distribution is then explored and improved by comparative studies of gait recognition performance, which increases the recognition efficiency and the possible application in edge computing scenarios. Furthermore, a deep learning network is developed based on long short-term memory (LSTM) and residual units to extract deep features from multi-channel time-series gait data to boost recognition performance. Experimental results demonstrate that the proposed gait sensor system can be utilized for human activity recognition and user identification with accuracies of 97.9 % and 99.4 %, respectively. Finally, a gait-sensing-based fitness exercise monitoring system is constructed that can estimate calorie expenditure and distinguish between standard and non-standard fitness activities with an accuracy of 97.2 %. This work can be extended to various application scenarios such as security surveillance, health monitoring, and intelligent control, which provides a new ubiquitous self-powered sensing solution for the Internet of Things (IoT).

1. Introduction

The Internet of Things (IoT) and intelligent buildings have received massive interest with the fast developments of sensing and computing technologies [1]. Human gait data have plentiful information and unique biometric features for activity recognition and user identification, which empower vital capabilities such as security surveillance, health monitoring, and daily entertainment in intelligent home systems. There are various gait sensing techniques and systems. The optical-based gait sensing system is widely used with abundant gait features [2], such as a camera and laser sensor, but it violates privacy and is easily blocked by environmental disturbance, and is hard for continuous measurement. The wearable system, such as an accelerometer or a gyroscope, is an alternative solution to solve these problems. However, the data collected from them is not enough and accurate for gait recognition, and it is sometimes not easy and comfortable to wear on the body [3,4]. The floor-based system is durable against environmental factors and helps protect privacy, while it can capture gait data without affecting daily activities because of its inconspicuous form [5]. With numerous sensing devices constructing a sensing array, it can detect multiple gait metrics

for gait analysis and recognition. Still, as a promising gait sensing technique, the floor-based system remains challenging to develop one that is not only robust for continuous and user-friendly gait monitoring but also inexpensive, easy to manufacture, and low energy consumption.

Several transducing mechanisms are widely deployed for floor-based gait sensor systems, including piezoelectric [6], electromagnetic [7], electrostatic [8], and triboelectric [9]. Energy supply is one of the most significant issues. The battery is commonly used, but it is bulky and has low reliability with high maintenance requirements. Energy harvesting from motion is a potential approach since it generates and uses electrical power in reaction to mechanical movement [10]. When a physical stimulus is applied to a triboelectric nanogenerator (TENG), it is converted into an electrical signal by contact electrification and electrostatic induction. TENG is an effective approach for self-powered sensing [11,12] and energy harvesting [13] due to its benefits such as high power density[14], robust electrical production [15], high energy efficiency [16], good flexibility [17], and low cost [18]. The functionality of TENG as self-powered motion [19–22], pressure [23–25], and vibration [26–29] sensors has been thoroughly confirmed. Recent research further highlighs the versatility of TENG in various energy harvesting applications [30–32] due to its excellent output voltage at a wide bandwidth for transforming mechanical power into electricity. Since the development of TENG sensors by Wang in 2012 [33], numerous research groups have explored their potential in wearable systems and gait sensing devices [34]. Early efforts in TENG-based gait sensors, such as the work by Lin et al. [35] and Han et al. [36], focused on the energy harvesting potential and basic motion sensing capabilities. However, these initial attempts faced several challenges, including wearing discomfort, vulnerability to environmental disturbances, and limited recognition accuracy. Later advancements, as demonstrated by the research of Zhang et al. [37] and Zhang et al. [38], sought to improve these limitations by integrating flexible textile materials, developing more sophisticated data processing methods, and incorporating machine learning techniques for enhanced recognition accuracy. Despite these advancements in wearable TENG-based systems and gait-sensing devices, several challenges persist. Wearing comfort remains a concern, as does the sensor's vulnerability to environmental disturbances. Moreover, there is an ongoing need for efficient data processing methods and strategies to achieve high recognition accuracy while maintaining low power consumption.

By addressing these challenges and building upon the work of previous researchers, our proposed triboelectric gait sensor system aims to provide a more comfortable, robust, and accurate solution for human activity recognition and user identification in various applications. The sensor is designed with copper and polytetrafluoroethylene (PTFE) as triboelectric layers and operates based on the triboelectric effect. To better process data from the gait sensor array and analyze the temporal information, an improved deep learning network has been developed, which is called the deep residual dense bidirectional long short-term memory network (Residual Dense-BiLSTM). The experimental findings demonstrate that our system can successfully recognize 5-class human activities with 97.9 % accuracy and identify 8-class users with 99.4 % accuracy. The system also serves as a fitness exercise monitoring system that can distinguish between standard and non-standard fitness activities with an accuracy of 97.2 %. Furthermore, a single TENG-based sensor unit can produce approximately 80 V output voltage and maximum output power of 10.58 µW during random low-frequency gait movements (around 1–2 Hz). It allows continuous energy harvesting in the massive deployment scenario. In real large-scale deployment scenarios with a perfect power management circuit, it is calculated that energy from gait movements can be utilized for signal acquisition and gait recognition. The system has the merit of low cost, high durability, unintrusive, and can protect privacy security while measuring gait signals. The functionalities and benefits mentioned above of the TENG-based gait sensor system make it an attractive candidate for security and healthcare applications in the fields of intelligent buildings and IoT.

2. Results and discussion

2.1. TENG-based gait sensor system

A schematic diagram of the TENG-based gait sensor system is depicted in Fig. 1a. The system is embedded into a carpet, and the users walk onto it. The gait signal generated by each movement is gathered and utilized for activity recognition, user identification as well as energy harvesting. As shown in Fig. 1b and c, one of the contact surfaces is made of PTFE with a thin film of copper as an electrode. The other contact surface is copper foil. A single-layer unit of the sensor is connected and stacked vertically to formulate a sensor unit and works in the contact separation mode. Fig. 1d demonstrates the design of the module. The sensor array is designed and optimized by foot pressure distribution and experiments. The structure of four sensor units is utilized, where one is in the front, two in the middle, and one in the end. Fig. 1e shows a photograph of a TENG-based sensor integrated into the front of the sensing insole module as a sensing unit. Through this design, a general architecture of a triboelectric gait sensor system is conceptualized in Fig. 1f. The signal acquisition, processing, transmission, and analysis steps are enhanced by technical advances in self-powered sensing and energy harvesting, enabling applications for security surveillance, fitness monitoring, personal healthcare, and smart home scenarios.

2.2. Design and mechanism

As shown in Fig. 2a, the TENG-based gait sensor system comprises two functional subsystems on the right side, the triboelectric sensing system and the energy harvesting system, based on the gait sensor unit located on the left side. The sensing module includes signal acquisition and pre-processing, data analysis and gait recognition by deep learning network, and wireless transmission to the user interface. Furthermore, the subsystem of gait energy harvesting is made of a power management module with a rectifying circuit for energy conditioning and an energy storage part. In the large-scale deployment scenario with a perfect power management circuit, it is calculated that the energy can be supplied for intermittent data acquisition and gait recognition. The user interface is to view the results and broaden the usage scenarios.

The basic principle of the whole system is to covert human gait into contact and separation movement of corresponding two triboelectric layers. Subsequently, it can generate gait signals naturally without any batter-based sensors and can also provide the energy for data processing for activity recognition and energy harvesting. The mechanism of electricity production is shown in Fig. 2b, and the COMSOL simulation of potential distribution is conducted and illustrated in Fig. 2c. When PTFE and copper plates come into contact against one another by an applied force, the transmission of surface charge happens on the surface owing to the triboelectric effect and electrostatic induction. Specifically, since the capability to obtain electrons of PTFE is higher than copper from triboelectric series of materials, the PTFE layer is electrically charged negatively when in contact with each other. Thus, the potential difference between the two sides is formed and changed as the two layers separate. Whilst the periodic force is applied and the external circuit is connected, the produced electrons move back and forth between two plates thanks to the triboelectric charges. As a consequence, an alternating current signal is produced. Details in the mechanism and COMSOL simulation are demonstrated in Note S1, and the mechanism of the one-layer sensing unit is shown in Fig. S1.

2.3. Electrical and mechanical characterization

To evaluate the sensor performance, some key parameters such as sensitivity, measurement range, and stability are characterized on the experimental platform with a force gauge to measure the applied forces of the linear motor.

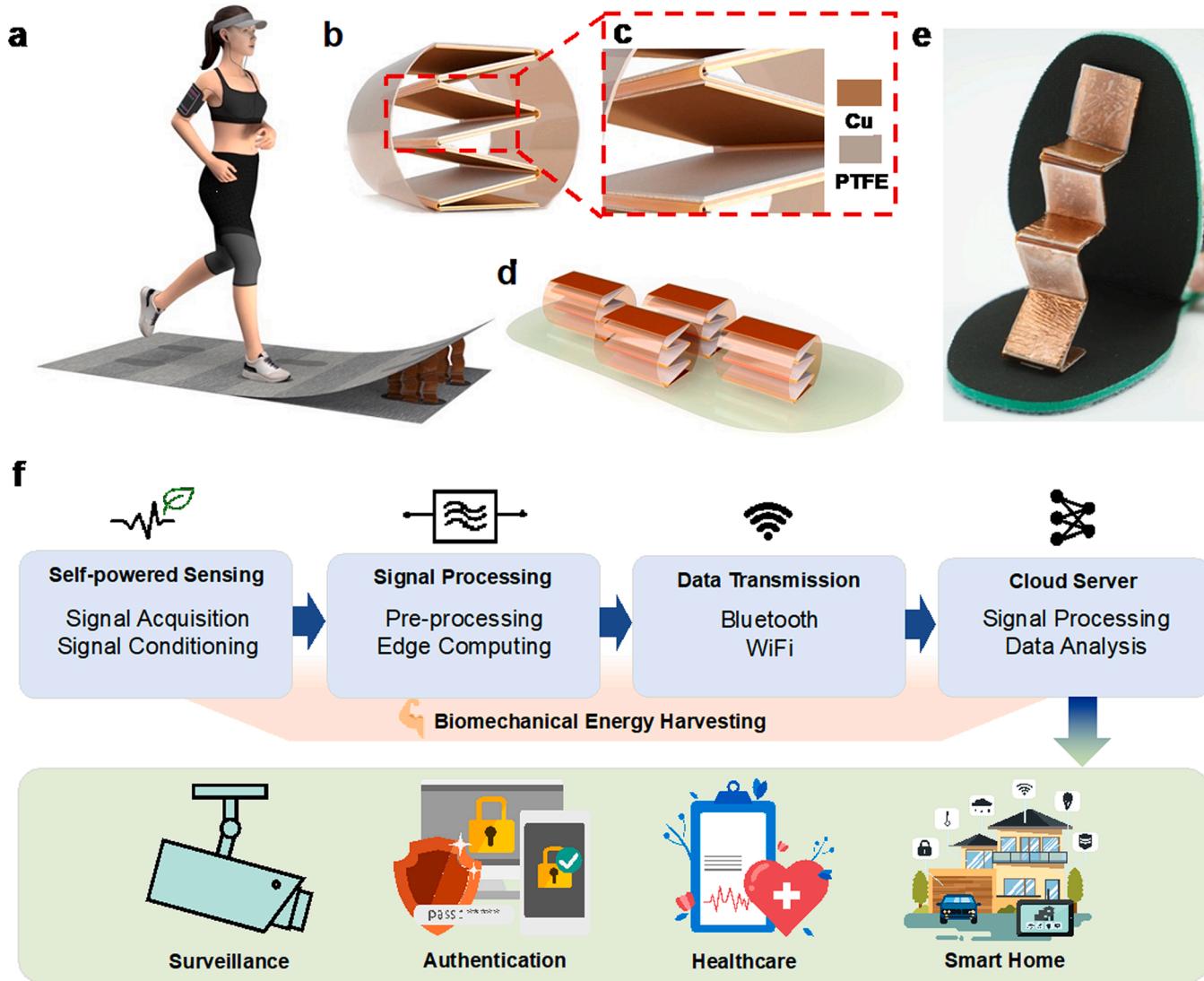The open-circuit voltage and short-circuit current responses are first

Fig. 1. System overview of the TENG-based gait sensor system for human activity recognition and user identification. (a) Schematic diagram of the gait sensor system. (b) Design of a six-layer TENG-based gait sensor. (c) Enlarged view of the sensor. (d) TENG-based smart sensing insole assembled with four gait sensors as a sensing array. (e) Photograph of a gait sensor integrated in the front of a smart sensing insole. (f) System overview of the gait sensor system.

studied with the force range set as 5 N to 30 N at a consistent frequency of 1 Hz, as shown in Fig. 3a and b. The open-circuit voltage outputs remain to stay around 80 V when the forces change from 5–30 N (Fig. 3a). Besides, there is a current output of around 0.25 μA with the force of 5 N and then keep increasing to the output of around 0.75 μA with the force of 30 N (Fig. 3b), indicating a decent sensing sensitivity. The constant voltage can be attributed to the total tribo-charges generated, which are proportional to the contact area between the two materials in the TENG sensor. As the force changes, the contact area remains relatively constant, resulting in a stable voltage output. On the other hand, when the contact force increases, it leads to more effective charge separation and faster contact-separation cycles, altering the rate of charge generation and results in a higher current output. Limitations in equipment, platform, and sensor monitoring range restricted our test scope to 30 N. Our sensor has a good rebound and shows decent sensitivity within the 30 N force range, implying that it is optimized for this specific range. Thus, a support structure is designed for actual human gait data collection in the gait sensor system to match the measurement range. Furthermore, the impact of operating frequencies on the sensor's output performance is also examined. Fig. 3c and Fig. 3d show that the open-circuit voltage and short-circuit current remain almost the same

with a constant force of 30 N at various working frequencies, which are around 80 V and 0.75 μA, respectively. It is because the contact duration between two layers of TENGs is similar when the linear motor is pressing with the same force at different operating frequencies. Thus, the transmitted charges are relatively constant, and the output stays the same.

To reduce the powerline frequency interference, a Butterworth low-pass filter is used. The sensor's output current, with a force of 30 N and a frequency of 1.5 Hz, is evaluated both with and without the filtering method. As shown in Fig. 3e, filtering help to decrease signal noise, which is helpful to the recognition accuracy in later steps. The sensor's response time to applied forces is also studied in order to analyze further the functionality of the sensor (Fig. 3f). The sensor was fixed, and the linear motor was in contact with the sensor to apply and remove the pressing force. The response time was measured as the interval between the force change and the corresponding open-circuit voltage change. The open-circuit voltage reveals a response time of less than 21 ms, identifying fast responses to an external force. The robustness of the sensor was evaluated by placing and removing a force a total of 3000 times. The open-circuit voltage and short-circuit current are shown in Fig. 3 g and h, which reflect the sensor's long-term stability and reliability. It is worth noting that the natural resilience of the zigzag
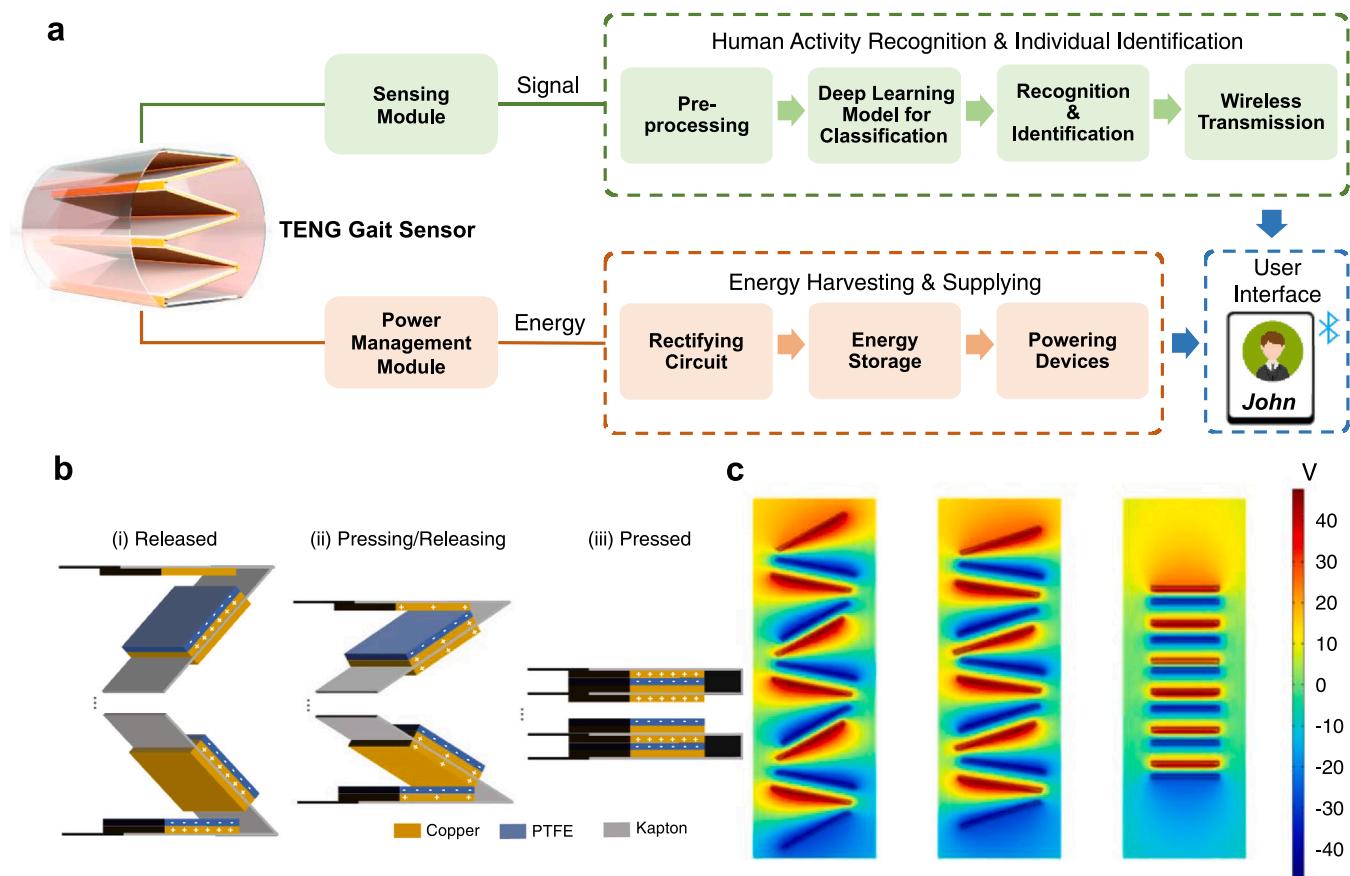
Fig. 2. Gait sensor system architecture and sensor working mechanism. (a) System architecture. (b) Schematic illustration of the working mechanism of a six-layer gait sensor. (c) Simulation results for the mechanism of potential distribution when two triboelectric layers are compressed in different levels.

structure is not perfect. Consequently, as the force is applied fast and periodically and sometimes the sensor does not recover and separate completely, resulting in the asymmetric current signal.

Furthermore, the energy harvesting performance is demonstrated when charging resistors, including the peak values of voltage, current, and power at various loads. As shown in Fig. 3i and j, the maximum voltage increased as the resistance raised, while the current across the load exhibited the inverse trend. At a load resistance of 0.05 $G\Omega$, the maximum output power of 10.58 μW is achieved. The power density can be boosted further by adding more layers to the TENG-based unit. Besides, three capacitors with values of 0.22, 0.47, and 1 μF were used as energy storage elements in the power conditioning circuit, which is chosen by balancing energy storage requirements, charging time, and other real application considerations. A rectifying circuit is implemented as a power conditioning circuit to convert the AC generated by the TENG-based unit into DC using diodes, ensuring a stable and continuous power supply for the electronic components in the system. The rectifying circuit is connected with the energy storage component to store the harvesting energy into different capacitors. Fig. 3k illustrates the results of charging multiple capacitors. The average power of the data acquisition chip for the sensor system is 535 mW, with the voltage and average current input as 5 V and 107 mA. A piece of intelligent carpet is 50 cm × 50 cm and consists of two sensing insole modules with eight sensor units. In real application scenarios such as a building lobby or corridor, assume it has a perfect power management circuit, and 128 pieces of carpets are laid in 32 m^2 ground. In a relatively high flow of people situation where every second a person passes each carpet, it is calculated that the energy harvesting module can power one gait sensing process every 50 s

To conclude, the sensor shows good sensitivity, rapid response time,

and great stability, which demonstrate its usefulness for gait measurement. Since the current output can show a good response to different applied forces, it is utilized as a key signal in data acquisition for the system instead of voltage output. At the same time, it can harvest power from the gait movements and store the energy in capacitors.

2.4. Optimization of sensing module

To improve the sensor design, the influence of the sensing layer on the performance of the sensor is first evaluated. A sensing layer unit stands for a single TENG-based sensing unit with one piece of copper and PTFE layer and can work in contact separation mode independently. As Fig. 4g shows, the sensors are fabricated by three to six units of sensing layers, respectively. The detailed fabrication process is stated in the method section. The linear motor is used to simulate the individual stepping with different speeds and acceleration on the sensor. The experimental results are presented in Fig. 4a, b, and c. The original sensor response of a = 3 m/s^2 and v = 0.2 m/s, a = 5 m/s^2 and v = 0.2 m/s, as well as a = 5 m/s^2 and v = 0.4 m/s with three to six sensing layers are shown in Fig. 4a, b, and c separately. The Fig. 4a and b is to explore how the difference of acceleration effect the sensing performance, and the Fig. 4b, and c is to explore how the difference of velocity affects the sensing performance. The open-circuit voltage outputs of the 6-layer and 5-layer sensors increase as the acceleration and velocity increase, while the 4-layer and 3-layer sensors remain almost the same. The increased voltage output can be attributed to the enhanced mechanical deformation of the TENG layers caused by the higher acceleration and velocity. This enhanced mechanical deformation leads to better contact and separation between the layers, resulting in more efficient charge transfer and increased voltage output. This
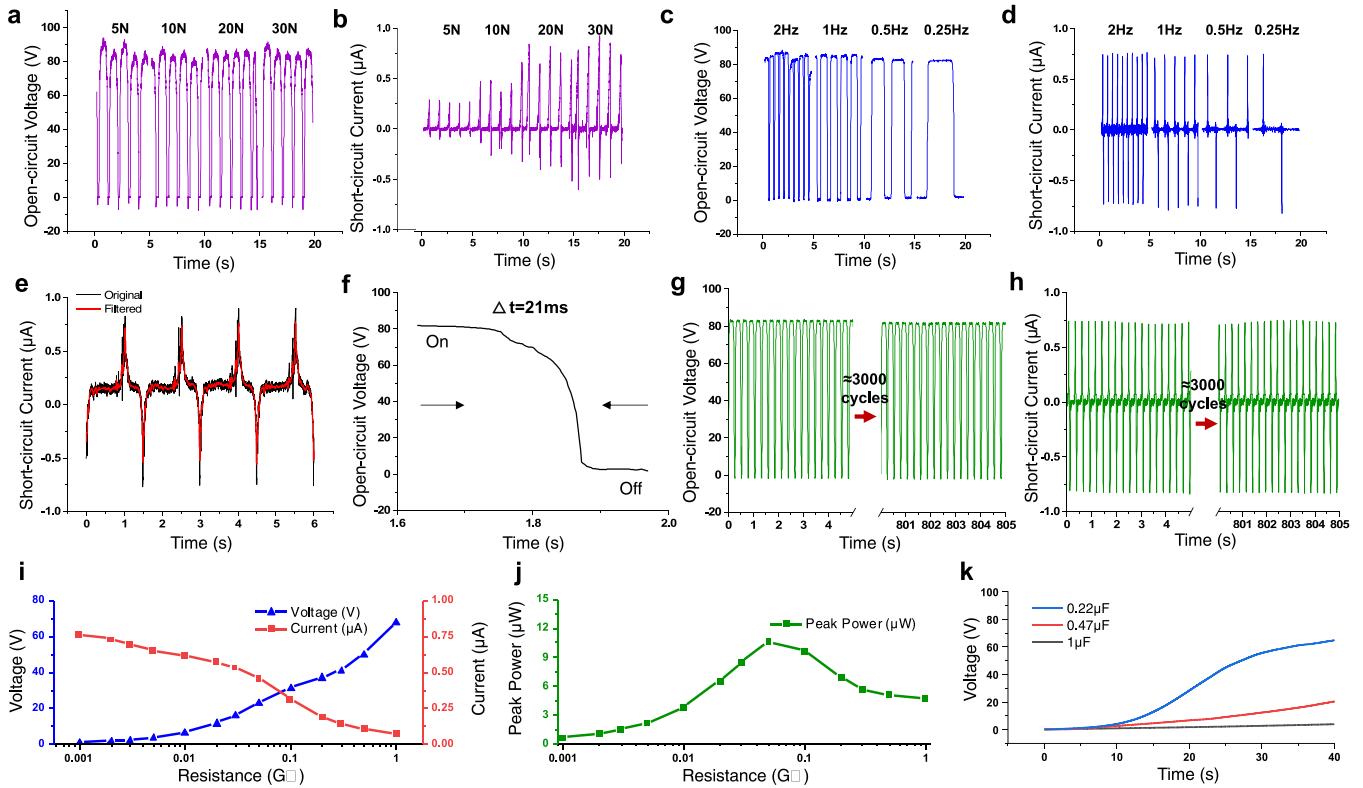
Fig. 3. Electrical and mechanical characterization of the gait sensor. (a) Open-circuit voltage and (b) Short-circuit current at various applied forces. (c) Voltage output and (d) Current output of the sensor at various pressing frequencies. (e) Comparison of the output signals with and without filtering. (f) Time response of the voltage in one cycle (external force of 30 N applied and released: on and off). (g) Open-circuit voltage and (h) short-circuit current to test the mechanical durability characterization of the TENG-based sensor in ≈ 3000 continuous working cycles with the force of 30 N. (i) Voltage and current of different resistance loads. (j) Peak power of different resistance loads on the performance of energy harvesting. (k) Voltage of charging different capacitors.

effect is more pronounced in the 6-layer and 5-layer sensors due to the increased number of layers providing more opportunities for contact and separation compared to the 4-layer and 3-layer sensors, which better helps distinguish different gait movements in further analysis. The figures show that all of the sensors can generate relatively consistent outputs. They show similar rapid responses to the start and end of the motion, which means they have a similar sensitivity. The sensor with six sensing layers produces the highest voltage output so that it can have a better signal amplitude and resolution than others. Besides, the energy harvesting performance will also be better. To balance the thickness of the sensor and the performance, sensors with more than six sensing layers are not considered. Thus, the sensor with six sensing layers is chosen as the major sensing device in the TENG-based gait sensor system.

The TENG-based gait sensor system is made up of a series of sensing insole modules, which are evenly distributed on the carpet in reference to human stride size. To better measure gait signals, the exploration of insole design is conducted. Based on the research on the distribution of pressure density and the spatial gait factors, the front and end of the sensing insole are implemented with some sensor units. To further measure gait signals and harvest energy, additional sensor units are placed in the middle of sensing insoles. For the insole with six sensors, there are three sensing groups separately put on the front, middle, and end of the insole to locate and monitor each part of the foot pressure (Fig. 4h (i)). Each sensing group contains two parallel sensor units. For the insole with four sensors, the front and back sensing groups are reduced by one sensor each (Fig. 4h (ii)). Specifically, two sensors are located at the front and end of the insole to maintain performance. The two sensors from the middle group are retained. For the insole with two sensors, the middle group is removed with two sensors eliminated (Fig. 4 h (iii)). Fig. 4d, e, and f illustrate the sample current outputs of

walking simulation in three sensing insoles with six, four, and two channels, separately. The data is pre-processed, and a simple LSTM model is utilized to evaluate the insoles by classifying different activities. The model results are demonstrated in Fig. 4i. The accuracy comes down, and the model size gets small when the number of channels decreases, which is because the information collected is reduced and the number of model parameters is decreased. However, the difference in accuracy and model size among different models are small, while the processing time of the 4-channel model is the minimum. To ensure the possibility of edge computing and large-scale deployment, a sensing insole with four sensor units is chosen for the gait sensor system.

2.5. Experiments and signal acquisition

The TENG-based gait sensor system consists of two sensing insole modules, each with four sensors. These modules are incorporated into the modular square carpet and measured by a portable data acquisition system (Fig. 5b). To accurately capture human gait patterns, the distance between the sensing insole modules is determined based on the standard gait model parameters and the convenience for real deployment scenarios, where the design stride length and step width are 100 cm and 10 cm, respectively. The sensing insole modules are evenly distributed on the carpet concerning these dimensions, ensuring accurate measurement of gait signals for various users. The data-acquisition circuit integrates the functions of data collection, data pre-processing, and wireless communication and has the advantages of being portable, lightweight, and low power consumption. The schematic diagram of the printed circuit board (PCB) is illustrated in Figs. S2 and S3, and the components and bills of materials are listed in Table S2. Users press on the sensing insole modules while walking and doing fitness exercises on the smart carpet, as illustrated in Fig. 5a. The system collects the gait
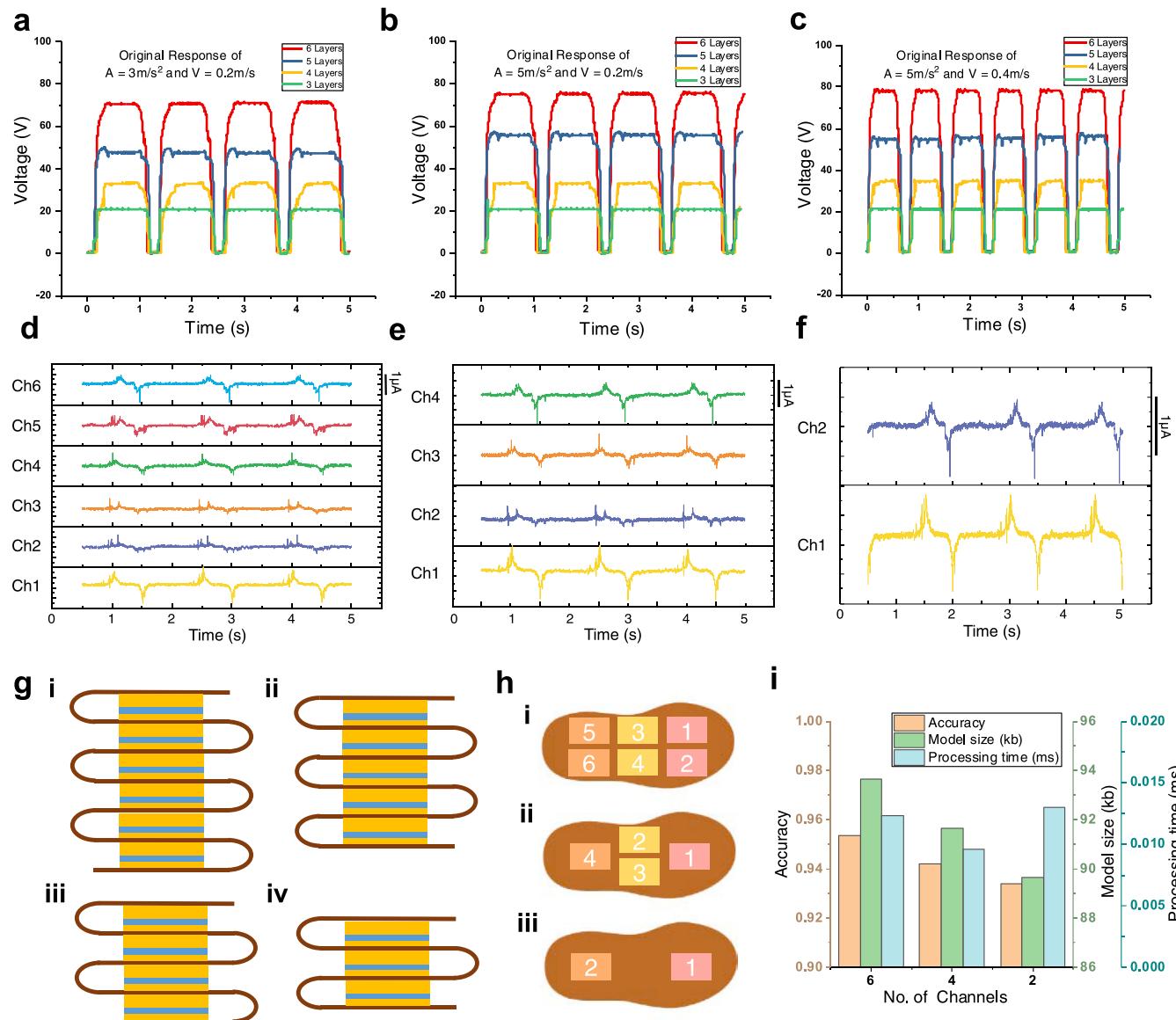
Fig. 4. Experiment and analysis of the sensor and insole design. (a-c) Voltage output of six, five, four, and three layer units on a TENG-based sensor on different acceleration and velocity. (a) A = 3 m/s² and V = 0.2 m/s, (b) A = 5 m/s² and V = 0.2 m/s, (c) A = 5 m/s² and V = 0.4 m/s. (d-f) Current output of (d) six, (e) four, (f) two channels on a smart sensing insole. (g) Design of a single TENG-based sensor with (i) six-layer, (ii) five-layer, (iii) four-layer, (iv) three-layer units. (h) Design of a smart sensing insole with (i) six, (ii) four, and (iii) two channels. (i) Accuracy, processing time, and model size of different smart sensing insoles' designs.

signal of five stepping activities, including standing, walking, jogging, running, and jumping, for human activity recognition. It also collects eight users' walking data for user identification. Fig. 5c illustrates an example of 8-channel current output for various users stepping on the sensors. The database includes a combination of eight users, and each user does five different activities separately, resulting in a total of 40 categories of data. For activity recognition, we combined the same action data for all 8 individuals and trained the deep learning network on this aggregated dataset. In contrast, for user identification, we only used walking data from each person separately and trained the network because the identity features are not obvious for standing and jogging or difficult to obtain accurately for the running and jumping activities. Each person's walking stride is unique, and the signal properties of various activities are diverse, providing special features for gait recognition.

The data acquisition and processing flow of the gait sensor system are demonstrated in Fig. 5e. The 8-channel current signals are wirelessly sent to the computer and then pre-processed by three steps, which are

stated in Note S2. Then, two separate deep learning networks are trained with labelled datasets and validated in the test dataset. A mobile app is designed as a user interface for users to receive and view the data from the gait sensor system, as illustrated in Fig. 5d. It is built on the Blynk IoT platform, an integrated IoT framework for developing and managing linked devices. It consists of three parts. The top part presents the signal from one of the two insole models. Each graph only shows one channel from the sensing insole due to the limited space where the front sensor is selected. The real-time sensing signal will be displayed in both graphs to monitor the system. The text information, such as classification results trained with the deep learning network, is described in the middle part. The bottom part shows pictures, such as the icons for various users and activities, to view the results more directly.

2.6. Design and demonstration of the system in gait recognition applications

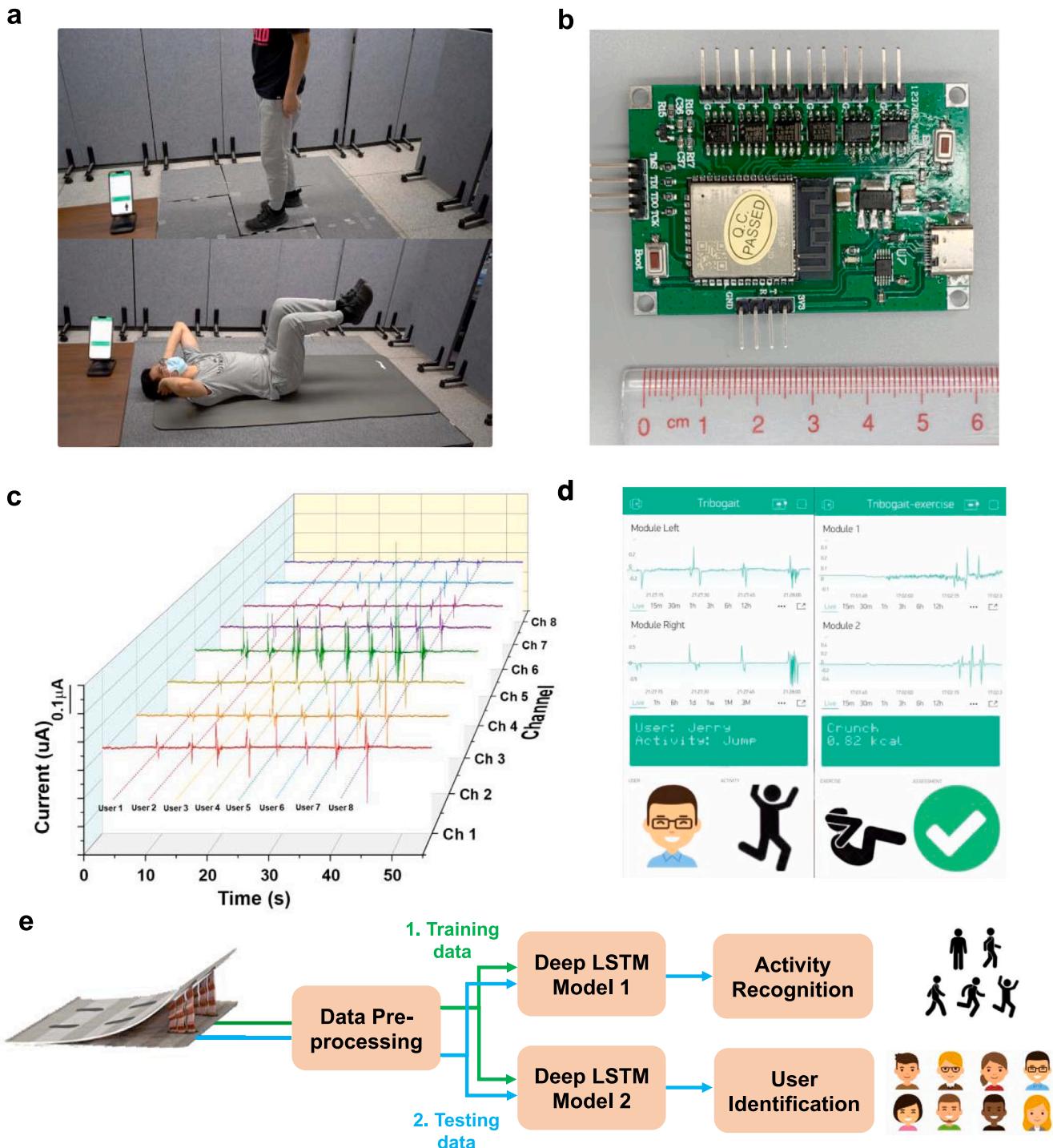A deep learning network called Residual Dense-BiLSTM is designed

Fig. 5. Experiments and evaluation of the gait sensor system. (a) Optical image of a user walking and doing fitness exercises on the system. (b) Image of a data acquisition system for portable data collection and wireless communication. (c) Sample eight-channel current output signals of eight different users collected by our system. (d) Mobile App for monitoring signals and viewing results. (e) Data flow of the gait sensor system for activity recognition and user identification.

and used for floor-based gait recognition, whose system diagram is shown in Fig. 6a. Its multilayer stacking structure help solve the multi-class time series gait recognition problem. The implementation detail is stated in the method section.

Fig. 6b and Fig. 6c depict the training of the deep learning algorithm for activity recognition. The results show that the proposed model can reach good classification accuracy and robustness as the training and testing accuracy and loss function converge. Following 500 training it-erations, the confusion matrix between predicted and true labels in the test dataset is displayed in Fig. 6f. With a prediction accuracy of up to

97.9 %, the TENG-based gait sensor system is able to distinguish be-tween a variety of activities. For user identification, the number of classes in the last layer of the model is altered from six to eight, and the rest of the training procedure is the same as described previously. Ac-curacy in both training and testing, as well as the loss function, converge as seen in Fig. 6d and e. After 500 epochs, the Fig. 6g confusion map shows that the model is able to attain a 99.4 % recognition rate. Compared to our previous work[12], here, a portable data acquisition chip is designed and used instead of an NI module as a centralized data acquisition system, which increases flexibility and decreases the cost of
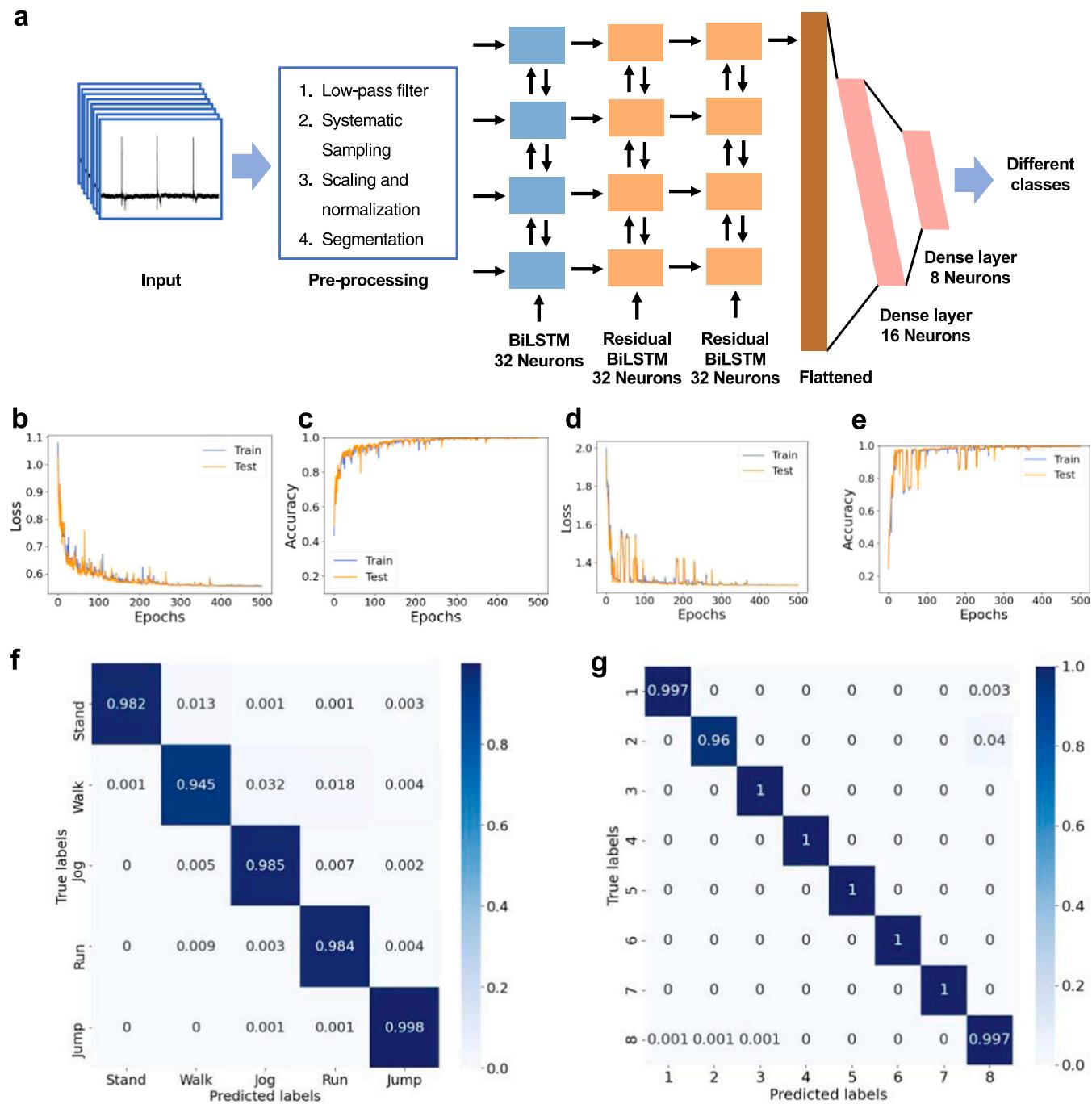
Fig. 6. Recognition model and results of the gait sensor system. (a) Proposed Residual Dense-BiLSTM network architecture for gait recognition. (b) Accuracy and (c) loss of the model training results for deep learning network monitoring. (d) Accuracy and (e) loss of the model training results for user identification. (f) Confusion matrix on the test dataset of deep learning network monitoring on five activities. (g) Confusion matrix on the test dataset of user identification on eight users.

large-scale wireless deployment. The parameters for data pre-processing and classifying algorithms are also finetuned. Because of the improvement in signal acquisition and analyzing methods, the data characteristics are a bit different, which leads to varied testing accuracies. The accuracy of user identification increases from 97.6 % to 99.4 %, while the accuracy of activity recognition decreases from 98.3 % to 97.9 %. In all, it illustrates a relatively higher performance than the previous floor-based gait sensor system, as Table S1 presents. The result reveals that the system can recognize human activities (see the Video S1) and identify users (see the Video S2) correspondingly.

Supplementary material related to this article can be found online at doi:10.1016/j.nanoen.2023.108473.

Supplementary material related to this article can be found online at doi:10.1016/j.nanoen.2023.108473.

Based on these, a fitness exercise recognition and monitoring system is built. Three fitness exercise activities (crunch, side crunch, and v-up) are used to validate the system performance. Data from those three activities are collected with a standard action and a non-standard action (only half the range of motion) separately. The model of three class standard activities is trained, and the test accuracy is 99.6 %. The three-class non-standard activities are considered as another three-class data to train a new model with six class data in total. Its testing accuracy is 97.2 %. The confusion matrixes are illustrated in Fig. S4. If the action is standard, according to the formula from Note S4 and the weight of the

user, the system can also estimate calories burned by counting the number of peaks. The fitness exercise application demo is shown in Video S3.

Supplementary material related to this article can be found online at doi:10.1016/j.nanoen.2023.108473.

3. Conclusion

In summary, a TENG-based gait sensor system is proposed, and an improved deep learning network is designed for multichannel gait recognition. The TENG-based sensor unit is designed, and the structure is improved to achieve better sensing resolution. Furthermore, the sensing array is built from the foot pressure model, and the sensor distribution is optimized to reach higher sensing efficiency. Meanwhile, the algorithm contains LSTM and residual network allows the system to dig more time series information from gait data. The system performs well in recognizing activities and identifying users, with accuracies of 97.9 % and 99.4 %, respectively. A fitness exercise monitoring system is also designed, and it can discriminate between various standard and non-standard fitness activities with a 97.2 % accuracy and estimate calorie expenditure, which broadens the health monitoring applications of the self-powered sensor. It can also function as an energy harvester, as shown by the charging of various load resistances and capacitors. The TENG-based gait sensor system can recognize gait movements with high accuracy and is appropriate for large-scale deployment and mass production. It is inexpensive, and simple to manufacture, which offers a wide variety of applications in security surveillance, health monitoring, and intelligent control.

4. Methods

4.1. Fabrication of the TENG-based gait sensor

The substrate is a piece of Kapton film with a size measuring 3.0 by 5.0 centimeters and 150 micrometers in thickness. By applying uniform deformations, the Kapton film is bent into a zigzag pattern. Both sides of the Kapton film can be used with TENG-based operating units owing to the zigzag design. Thin film PTFE and copper foil make up the front/ contact electrode. Another thin copper film is applied as the backside electrode on the other side. In particular, the front electrode of each layer is constructed by adhering 60 micrometers of copper to the substrate using 1-millimeter thick 3 M foam tapes. Next, the surface of the copper on the other side is left exposed while a thin PTFE layer adheres over it. A copper foil is taped to the backside to form the backside electrode. The parallel connections between the various levels are made using copper cables. A striped Kapton surrounds the single TENG-based sensor, compacting the zigzagging layered structure and fastening it together. It can harvest power from both pushing and twisting, thanks to its flexibility and moderate rigidity.

4.2. Characterization and measurement

An experimental platform with a linear motor is built for sensor characterization and exploration of the sensing insole. It can provide different accelerations and velocities to simulate situations for users with various weights and velocities when stepping onto it. It is also used to simulate different kinds of stepping activities, such as standing, walking, and running. The sensor performance is evaluated by voltage and current output and measured by a Keithley 6514 electrometer. A NI cDAQ-9174 chassis is utilized to collect the multichannel signal data for the sensing insole and the whole gait sensor system. When collecting data on people actually walking through, a 10 MΩ resistance is wired in series with each sensor to prevent damage to the device and provide a stable signal. The display of the characterization and measurement system is built-in LabVIEW. Furthermore, a portable data acquisition chip is designed to collect and transmit data wirelessly for practical application scenarios and large-scale deployments.

4.3. Deep learning network and training process

The Residual Dense-BiLSTM model first integrates multiple LSTM (long short-term memory) layers to collect more temporal information, including BiLSTM [39] and Residual BiLSTM [40], where residual architecture help overcome the issue of gradients vanishing. Then, several fully connected layers are stacked to enhance feature propagation [41].

There are a series of functional layers in the model. Because the system records a time series of data from many gait channels, it is essential that the training data be prepared in accordance with the LSTM's requirements for both the training and evaluation process. In order to accommodate the LSTM, the model first turns the eight separate 1-D time series data into a 3-D structure. It combines the information and setup of the total number of sensor channels, batch sizes, and memory steps. The next layer, called the bidirectional input layer, is made up of 32 neurons. These neurons learn from the information in the preceding layers. Additionally, the model includes a stack of two residual BiLSTM layers to account for a deeper temporal dependency when forecasting the subsequent value. Two dense layers with 16 and 8 neurons were employed as the fully connected and output layers to help categorize features. Moreover, the SoftMax function is used to manage the multi-class classifying problem. To avoid overfitting and boost network generalization, LSTM networks include a dropout component with probability. The algorithm is implemented with Pytorch [42] in Python and trained offline on a GeForce RTX 3090 GPU running on an Ubuntu server using an Adam optimizer set to a learning rate of 0.0015.

CRediT authorship contribution statement

W. Ding guided the project. W. Ding, J. Wang, J. Li, Z. Xie, Z. Wang designed and conducted the experiment; J. Li wrote the original draft. All authors discussed the results and reviewed the manuscript.

Declaration of Competing Interest

The authors declare that they have no known competing financial interests or personal relationships that could have appeared to influence the work reported in this paper.

Data Availability

Data will be made available on request.

Appendix A. Supporting information

Supplementary data associated with this article can be found in the online version at doi:10.1016/j.nanoen.2023.108473.

References

[1] D. Minoli, K. Sohraby, B. Occhiogrosso, IoT considerations, requirements, and architectures for smart buildings—energy optimization and next-generation building management systems, IEEE Internet Things J. 4 (2017) 269–283.

[2] E. Stone, M. Skubic, Evaluation of an inexpensive depth camera for in-home gait assessment, J. Ambient Intell. Smart Environ. 3 (2011) 349–361.

[3] B.R. Greene, D. McGrath, R. O'Neill, K.J. O'Donovan, A. Burns, B. Caulfield, An adaptive gyroscope-based algorithm for temporal gait analysis, Med. Biol. Eng. Comput. 48 (2010) 1251–1260.

[4] Z. Wang, J. Li, Y. Jin, J. Wang, F. Yang, G. Li, W. Ni, W. Ding, Sensing beyond itself: multi-functional use of ubiquitous signals towards wearable applications, Digit. Signal Process. (2021), 103091.

[5] C. Brown Wilson, J.C. Ceballos, P. Wright, J. Vaughan, C. Todd, P.J. Scully, K. B. Ozanyan, Developing a sensing solution to reduce the risk of falls for older people: an interdisciplinary approach, Gerontechnology 13 (2014).

[6] H.S. Kim, J.-H. Kim, J. Kim, A review of piezoelectric energy harvesting based on vibration, Int. J. Precis. Eng. Manuf. 12 (2011) 1129–1141.

[7] B. Yang, C. Lee, W. Xiang, J. Xie, J. Han, He, R.K. Kotlanka, S.P. Low, H. Feng, Electromagnetic energy harvesting from vibrations of multiple frequencies, J. Micromech. Microeng. 19 (2009), 035001.

[8] S. Boisseau, G. Despesse, B. Ahmed, Small-scale energy harvesting, InTech (2012).

[9] A. Ahmed, I. Hassan, M.F. El-Kady, A. Radhi, C.K. Jeong, P.R. Selvaganapathy, J. Zu, S. Ren, Q. Wang, R.B. Kaner, Integrated triboelectric nanogenerators in the era of the internet of things, Adv. Sci. (Weinh.) 6 (2019), 1802230-1802230.

[10] P.D. Mitcheson, E.M. Yeatman, G.K. Rao, A.S. Holmes, T.C. Green, Energy harvesting from human and machine motion for wireless electronic devices, Proc. IEEE 96 (2008) 1457–1486.

[11] C. Wu, W. Ding, R. Liu, J. Wang, A.C. Wang, J. Wang, S. Li, Y. Zi, Z.L. Wang, Keystroke dynamics enabled authentication and identification using triboelectric nanogenerator array, Mater. Today 21 (2018) 216–222.

[12] J. Li, Z. Wang, Z. Zhao, Y. Jin, J. Yin, S.-L. Huang, J. Wang, TriboGait: a deep learning enabled triboelectric gait sensor system for human activity recognition and individual identification, Adjun. Proc. 2021 ACM Int. Jt. Conf. Pervasive Ubiquitous Comput. Proc. 2021 ACM Int. Symp. Wearable Comput. (2021) 643–648.

[13] J. Chen, Y. Huang, N. Zhang, H. Zou, R. Liu, C. Tao, X. Fan, Z.L. Wang, Micro-cable structured textile for simultaneously harvesting solar and mechanical energy, Nat. Energy 1 (2016).

[14] H. Wu, S. Wang, Z. Wang, Y. Zi, Achieving ultrahigh instantaneous power density of 10 MW/m2 by leveraging the opposite-charge-enhanced transistor-like triboelectric nanogenerator (OCT-TENG), Nat. Commun. 12 (2021) 5470.

[15] Z. Lin, B. Zhang, H. Guo, Z. Wu, H. Zou, J. Yang, Z.L. Wang, Super-robust and frequency-multiplied triboelectric nanogenerator for efficient harvesting water and wind energy, Nano Energy 64 (2019), 103908.

[16] S. Liu, X. Liu, G. Zhou, F. Qin, M. Jing, L. Li, W. Song, Z. Sun, A high-efficiency bioinspired photoelectric-electromechanical integrated nanogenerator, Nat. Commun. 11 (2020) 6158.

[17] R. Liu, X. Kuang, J. Deng, Y.-C. Wang, A.C. Wang, W. Ding, Y.-C. Lai, J. Chen, P. Wang, Z. Lin, H.J. Qi, B. Sun, Z.L. Wang, Shape Memory Polymers for Body Motion Energy Harvesting and Self-Powered Mechanosensing, Adv. Mater. 30 (2018) 1705195.

[18] W. Ding, J. Zhou, J. Cheng, Z. Wang, H. Guo, C. Wu, S. Xu, Z. Wu, X. Xie, Z. L. Wang, TriboPump: a low-cost, hand-powered water disinfection system, Adv. Energy Mater. 9 (2019) 1901320.

[19] F. Yi, L. Lin, S. Niu, J. Yang, W. Wu, S. Wang, Q. Liao, Y. Zhang, Z.L. Wang, Self-powered trajectory, velocity, and acceleration tracking of a moving object/body using a triboelectric sensor, Adv. Funct. Mater. 24 (2014) 7488–7494.

[20] Y.S. Zhou, G. Zhu, S. Niu, Y. Liu, P. Bai, Q. Jing, Z.L. Wang, Nanometer resolution self-powered static and dynamic motion sensor based on micro-grated triboelectrification, Adv. Mater. 26 (2013) 1719–1724.

[21] W. Yang, J. Chen, X. Wen, Q. Jing, J. Yang, Y. Su, G. Zhu, W. Wu, Z.L. Wang, Triboelectrification based motion sensor for human-machine interfacing, ACS Appl. Mater. Interfaces 6 (2014) 7479–7484.

[22] H. Guo, X. Jia, L. Liu, X. Cao, N. Wang, Z.L. Wang, Freestanding triboelectric nanogenerator enables noncontact motion-tracking and positioning, ACS nano 12 (2018) 3461–3467.

[23] P.-K. Yang, Z.-H. Lin, K.C. Pradel, L. Lin, X. Li, X. Wen, J.-H. He, Z.L. Wang, Paper-based origami triboelectric nanogenerators and self-powered pressure sensors, ACS Nano 9 (2015) 901–907.

[24] J. Luo, F.R. Fan, T. Zhou, W. Tang, F. Xue, Z.L. Wang, Ultrasensitive self-powered pressure sensing system, Extrem. Mech. Lett. 2 (2015) 28–36.

[25] X. Wang, M. Que, M. Chen, X. Han, X. Li, C. Pan, Z.L. Wang, Full dynamic-range pressure sensor matrix based on optical and electrical dual-mode sensing, Adv. Mater. 29 (2017).

[26] X. Fan, J. Chen, J. Yang, P. Bai, Z. Li, Z.L. Wang, Ultrathin, rollable, paper-based triboelectric nanogenerator for acoustic energy harvesting and self-powered sound recording, ACS Nano 9 (2015) 4236–4243.

[27] W. Li, D. Torres, R.Æ. D®™az, Z. Wang, C. Wu, C. Wang, Z. Lin Wang, N. Sep®≤lveda, Nanogenerator-based dual-functional and self-powered thin patch loudspeaker or microphone for flexible electronics, Nat. Commun. 8 (2017).

[28] H. Guo, X. Pu, J. Chen, Y. Meng, M.-H. Yeh, G. Liu, Q. Tang, B. Chen, D. Liu, S. Qi, C. Wu, C. Hu, J. Wang, Z.L. Wang, A highly sensitive, self-powered triboelectric auditory sensor for social robotics and hearing aids, Sci. Robot. 3 (2018) eaat2516.

[29] N. Arora, S.L. Zhang, F. Shahmiri, D. Osorio, Y.-C. Wang, M. Gupta, Z. Wang, T. Starner, Z.L. Wang, G.D. Abowd, SATURN, Proceedings of the ACM on Interactive, Mobile Wearable Ubiquitous Technol. 2 (2018) 1–28.

[30] F.-R. Fan, L. Lin, G. Zhu, W. Wu, R. Zhang, Z.L. Wang, Transparent triboelectric nanogenerators and self-powered pressure sensors based on micropatterned plastic films, Nano Lett. 12 (2012) 3109–3114.

[31] C. Han, C. Zhang, W. Tang, X. Li, Z.L. Wang, High power triboelectric nanogenerator based on printed circuit board (PCB) technology, Nano Res. 8 (2014) 722–730.

[32] Y. Xi, H. Guo, Y. Zi, X. Li, J. Wang, J. Deng, S. Li, C. Hu, X. Cao, Z.L. Wang, Multifunctional TENG for blue energy scavenging and self-powered wind-speed sensor, Adv. Energy Mater. 7 (2017) 1602397.

[33] Z.L. Wang, Triboelectric nanogenerators as new energy technology for self-powered systems and as active mechanical and chemical sensors, ACS Nano 7 (2013) 9533–9557.

[34] Q. Li, K. Dai, W. Zhang, X. Wang, Z. You, H. Zhang, Triboelectric nanogenerator-based wearable electronic devices and systems: Toward informatization and intelligence, Digit. Signal Process. 113 (2021), 103038.

[35] Z. Lin, Z. Wu, B. Zhang, Y.-C. Wang, H. Guo, G. Liu, C. Chen, Y. Chen, J. Yang, Z. L. Wang, A triboelectric nanogenerator-based smart insole for multifunctional gait monitoring, Adv. Mater. Technol. 4 (2018) 1800360.

[36] Y. Han, F. Yi, C. Jiang, K. Dai, Y. Xu, X. Wang, Z. You, Self-powered gait pattern-based identity recognition by a soft and stretchable triboelectric band, Nano Energy 56 (2019) 516–523.

[37] Z. Zhang, T. He, M. Zhu, Z. Sun, Q. Shi, J. Zhu, B. Dong, M.R. Yuce, C. Lee, Deep learning-enabled triboelectric smart socks for IoT-based gait analysis and VR applications, npj Flex. Electron. 4 (2020).

[38] Q. Zhang, T. Jin, J. Cai, L. Xu, T. He, T. Wang, Y. Tian, L. Li, Y. Peng, C. Lee, Wearable triboelectric sensors enabled gait analysis and waist motion capture for Iot-based smart healthcare applications, Adv. Sci. (Weinh.) 9 (2022) (cs).

[39] M. Schuster, K.K. Paliwal, Bidirectional recurrent neural networks, IEEE Trans. Signal Process. 45 (1997) 2673–2681.

[40] Y. Zhao, R. Yang, G. Chevalier, X. Xu, Z. Zhang, Deep residual bidir-LSTM for human activity recognition using wearable sensors, Math. Probl. Eng. 2018 (2018) 1–13.

[41] J. Zhang, F. Wu, B. Wei, Q. Zhang, H. Huang, S.W. Shah, J. Cheng, Data augmentation and dense-LSTM for human activity recognition using WiFi signal, IEEE Internet Things J. 8 (2021) 4628–4641.

[42] A. Paszke, S. Gross, F. Massa, A. Lerer, J. Bradbury, G. Chanan, T. Killeen, Z. Lin, N. Gimelshein, L. Antiga, Pytorch: an imperative style, high-performance deep learning library, Adv. Neural Inf. Process. Syst. 32 (2019).